Available online at www.sciencedirect.com
SCIENCE DIRECT®

Journal of the European Ceramic Society 24 (2004) 1343–1347

www.elsevier.com/locate/jeurceramsoc

The polarization of mixed conducting SOFC cathodes: Effects of surface reaction coefficient, ionic conductivity and geometry

J. Fleig*, J. Maier

Max-Planck-Institute for Solid State Research, Heisenbergstr. 1, 70569 Stuttgart, Germany

Abstract

Multi-dimensional finite element simulations of current distributions in mixed ionic and electronic conducting cathodes (MIEC) are presented for the case that the cathodic oxygen incorporation into an electrolyte takes place through the bulk of the electrode. The effects of the ionic conductivity and the surface reaction coefficient on the overall process are analyzed. Depending on these material parameters different parts of the cathode are involved in the oxide ion transport to the electrolyte (from a very small region close to the three phase boundary for a fast surface reaction up to the entire cathode for a very slow surface reaction). The calculations also reveal which combinations of ionic conductivity and surface reaction coefficient are appropriate to achieve acceptable polarization resistances. The influence of the particle size is discussed and interpolation formulae are given to estimate the cathodic polarization in porous MIECs.

Keywords: Diffusion; Fuel cells; Ionic conductivity; Polarization resistance

1. Introduction

The electrochemical performance of a solid oxide fuel cell (SOFC) strongly depends on the kinetics of the cathodic oxygen reduction reaction. Mixed electronic and ionic conducting cathodes (MIECs) facilitate an oxygen reduction and incorporation in the electrolyte not only via a surface path (oxygen adsorption, dissociation, surface diffusion to the three phase boundary, ionization and incorporation into the electrolyte) but also via a bulk path: oxygen can be adsorbed and ionized on the MIEC surface and incorporated into the cathode; under electric load the oxide ions then diffuse through the cathode bulk and are transferred into the electrolyte at the interface between electrode and electrolyte.[1–5] This bulk path might considerably lower the polarization resistance of SOFCs if the material and geometrical parameters of the MIEC are chosen properly. Theoretical tools are therefore highly desired that allow one to predict the effects of the relevant parameters on the polarization resistance.

Most calculations dealing with the polarization resistance of MIECs are based on one-dimensional considerations[6–8] and therefore have a restricted validity range. Recently, simulations of the two-dimensional current distribution in mixed conducting cathode particles have been presented for the case that transport of oxide ions in the cathode bulk is rate-limiting.[9] It has, for example, been discussed whether or not the electrochemically active zone of the cathode broadens if the ionic conductivity of the electrode is enhanced. In this contribution we extend these calculations to cases in which the oxygen incorporation into the cathode significantly influences the overall reaction rate. In particular the relation between geometry and polarization resistance is discussed for different material parameters.

2. Model system and theoretical considerations

The two model geometries considered are shown in Fig. 1. The first model cathode consists of "pillars" of 50 cylindrical-shaped mixed conducting particles (particle diameter L_p, particle height L_p, "pillar" height $h = 50\ L_p$, distance between two "pillars" $= 2L_p$, Fig. 1a and c). In a second cathode every second "particle" is thickened thus representing the "cross-beams" which lead to the three-dimensional, percolating topology of a porous SOFC cathode (Fig. 1b and d). The entire side

* Corresponding author. Tel.: +49-711-689-1770; fax: +49-711-689-1722.
E-mail address: j.fleig@fkf.mpg.de (J. Fleig).

0955-2219/$ - see front matter © 2003 Elsevier Ltd. All rights reserved.
doi:10.1016/S0955-2219(03)00561-2

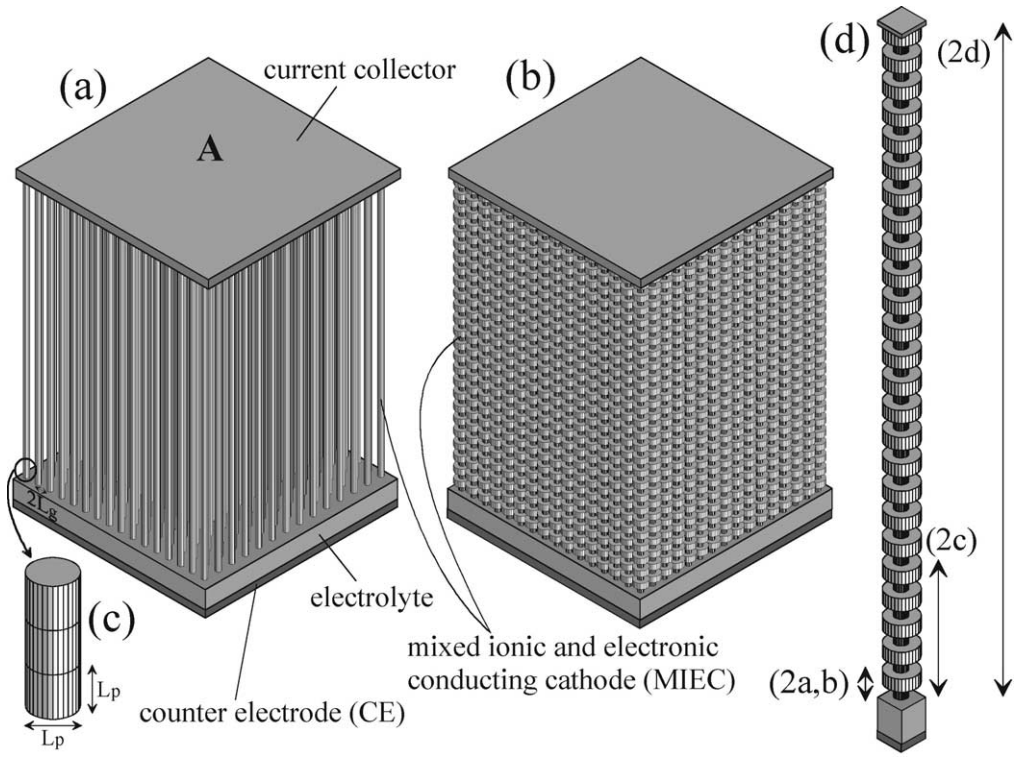

Fig. 1. (a) and (b): Sketches of the two model geometries (A and B) under consideration. (c) Magnification of three particles of the mixed conducting cathode of geometry A. (d) Unit element of geometry B; for the sake of simplicity a cylindrically shaped electrolyte is used in the calculations. The three arrows indicate the fractions of the unit element for which the potential distributions are plotted in Fig. 2.

walls of the "pillars" are assumed to be electrochemically active. Owing to symmetry only a unit element (Fig. 2d) has to be considered in the calculations. It is further assumed that only the bulk path contributes to the overall oxygen reduction current and that two steps determine the electrochemical polarization, namely the oxygen reduction reaction at the surface of the cathode and the ionic transport through the MIEC. The surface step is described by an area-related resistance $\tilde{R}_k$ (in Ωcm^2) and can be converted into an electrical surface exchange coefficient k^q via $k^q = (kT)/(4e^2\tilde{R}_k c)$. (Symbol c denotes the oxide ion concentration and k, T, e are the Boltzmann constant, temperature and elementary charge, respectively.) The ionic transport in the bulk of the MIEC is determined by the ionic conductivity of the MIEC, σ_{ion}, which is related to the self diffusion coefficient D^q of oxide ions via the Nernst–Einstein equation $D^q = (kT\sigma_{ion})/(4e^2c)$. The electronic conductivity in the MIEC is assumed to be so large that only a negligible gradient of the electrochemical potential of the electrons is required to enable the electronic current to flow from the current collector which covers the top of the cathode to the free surfaces of the cathode ($MIEC_{fs}$). As discussed in Ref. [9] div(grad $\tilde{\mu}_V$) = 0 has therefore to be solved under the boundary conditions $\nabla_n\tilde{\mu}_V(MIEC_{fs}) = \tilde{R}_k^{-1}\sigma_{ion}^{-1}(2eU - \tilde{\mu}_V(MIEC_{fs}))$ and $\tilde{\mu}_V(CE) = 0$ in order to obtain the electrochemical potential of oxygen vacancies ($\tilde{\mu}_V$) in the sample. (CE denotes the reversible counter electrode, ∇_n is the gradient normal to the surface, U the applied voltage; the equilibrium electrochemical potential of vacancies is set to zero.) From $\nabla\tilde{\mu}_V$ the ionic current density and thus the polarization resistance can be calculated. Homogeneous σ_{ion}-values of 10^{-7}–10^{-3} S/cm are used and the electrolyte is regarded to be a pure ionic conductor with conductivity $\sigma_{IC} = 10^{-1}$ S/cm. Since $\sigma_{IC} \gg \sigma_{ion}$ the polarization resistance of the entire cell corresponds to the cathodic polarization resistance. The particle size L_p is varied from 500 nm to 4 μm and the height of the cathode is 50 L_p, i.e. between 25 and 200 μm while the electrolyte is $3L_p$ thin. The finite element package FLUXEXPERT (SIMULOG, France) was applied to numerically calculate $\tilde{\mu}_V$ and the area-related polarization resistance $\tilde{R}_{pol}$. More information on these calculations can be found in Ref. [9].

3. Results and discussion

Let us first consider the potential distributions in the model cathodes for different k^q and D^q (or $\tilde{R}_k^{-1}$ and σ_{ion}) values. Fig. 2 shows the $\tilde{\mu}_V$ distributions in geometry B

for four different cases: For a fast oxygen surface reaction (low $\tilde{R}_k$) the oxygen incorporation mainly occurs close to the three phase boundary (3PB) (see Fig. 2a); this situation has been discussed in depth in Ref. [9]. For a moderate surface reaction coefficient ($L_p k^q/D^q \approx 1$) the current-carrying region is broadened. However, it is still mainly the first particle layer which is involved in the oxygen reduction reaction (Fig. 2b): for $L_p k^q/D^q = 1$ more than 85% of the oxygen is incorporated at the surface of the particle layer that is in contact with the electrolyte. If the resistance of the oxygen surface reaction further increases, more and more particle layers contribute to the oxygen reduction reaction (Fig. 2c) and for very high $\tilde{R}_k$ values (Fig. 2d) the entire cathode is "active". The same considerations are also valid for geometry A.

Fig. 3a illustrates the dependence of the polarization resistance on the surface reaction resistance for $L_p = 1.6$ μm and $\sigma_{ion} = 10^{-3}$ S/cm. Four regimes can be distinguished and each of them corresponds to one of the potential distributions shown in Fig. 2: As long as $\tilde{R}_k$ is low, the polarization resistance is constant (regime I) and the oxygen incorporation into the MIEC occurs close to the 3PB (Fig. 2a). In regime II $\tilde{R}_{pol}$ becomes increasingly dependent on $\tilde{R}_k$ and the ionic current penetrates into the first particle layer (Fig. 2b). Regime III is characterized by the fact that more than one particle layer is involved in the oxygen reduction reaction (Fig. 2c) and yields, to a good approximation, a proportionality of $\tilde{R}_{pol}$ and $\sqrt{\tilde{R}_k}$. In regime IV, lastly, $\tilde{R}_{pol} \propto \tilde{R}_k$ results and the entire cathode surface is relevant with respect to the oxygen reduction reaction (Fig. 2d). For geometry B the resistances in regimes III and IV are somewhat lower than for geometry A which is not surprising since in these cases the larger surface area of cathode B decreases the polarization. In regimes I and II, however, only the particles in contact with the electrolyte are relevant and both geometries lead to the same results.

In Fig. 3b the influence of the ionic conductivity of the MIEC on the polarization resistance is shown for cathode A. As one might intuitively expect, the importance of σ_{ion} decreases with increasing $\tilde{R}_k$ (decreasing k^q): In regime I (cf. Fig. 3a) the transport of oxide ions in the MIEC is rate-determining and $\tilde{R}_{pol} \propto \sigma_{ion}^{-1}$ results while in regime IV σ_{ion} plays no role. The limits between

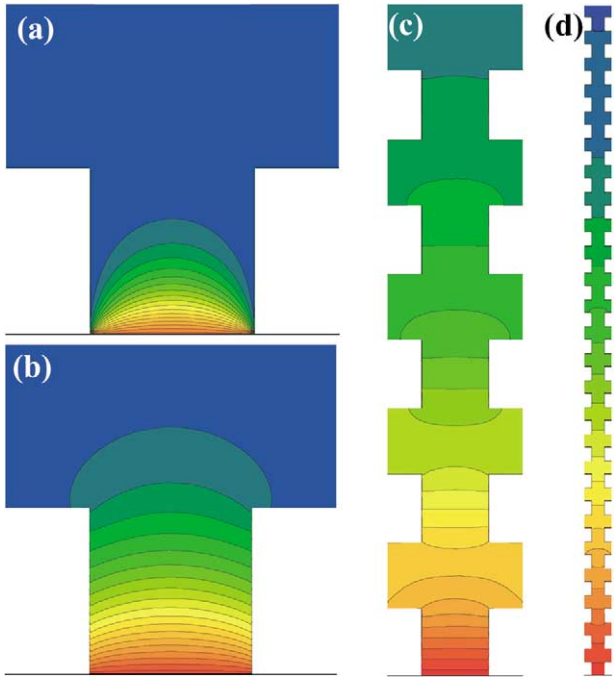

Fig. 2. Potential distributions of $\tilde{\mu}_V$ in parts of the cathode B for different $L_p k^q/D^q$ ($= L_p \tilde{R}_k^{-1}/\sigma_{ion}$) ratios: (a) 10^5, (b) 1, (c) 10^{-2} and (d) 10^{-7}; $L_p = 1.6$ μm, $\sigma_{ion} = 10^{-3}$ S/cm. The distributions are shown for cross sections of fractions of cathode geometry B; the corresponding fractions are indicated in Fig. 1d. Changes in the color correspond to equipotential lines, the current flows perpendicular to these lines. Obviously more and more of the cathode carries an ionic current if the $L_p k^q/D^q$-value decreases. The potential difference between two lines is 1/20 of the maximum potential difference occurring in the bulk of the cathode.

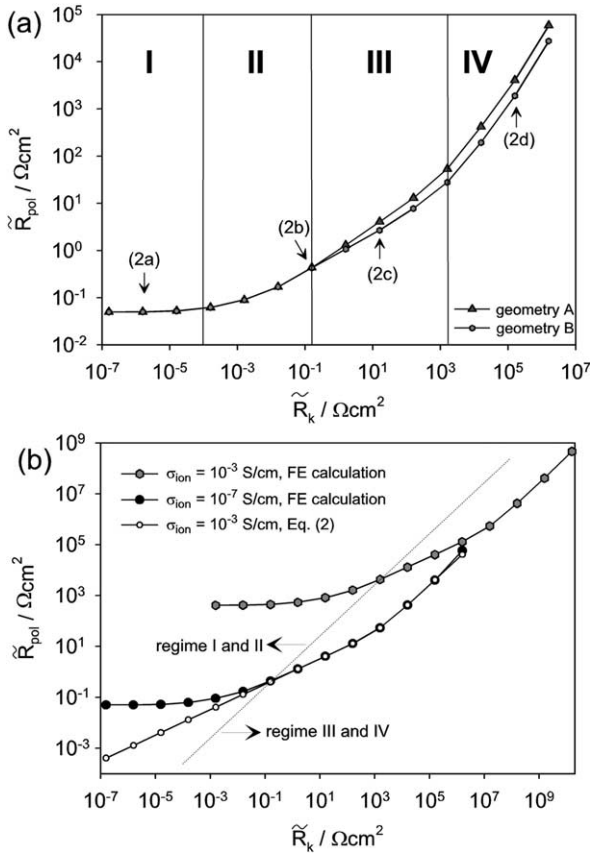

Fig. 3. (a) Area-related polarization resistance for different $\tilde{R}_k$-values and two geometries; $L_p = 1.6$ μm, $\sigma_{ion} = 10^{-3}$ S/cm. Four different regimes (I–IV) can be distinguished. Increasing $\tilde{R}_k$ leads to a decreasing density of equipotential lines (cf. Fig. 2). The data points which correspond to Fig. 2(a)–(d) are also indicated. (b) Area-related polarization resistance for different σ_{ion}-values (geometry A) and $\tilde{R}_{pol}$ calculated from Eq. (2); $L_p = 1.6$ μm, $\sigma_{ion} = 10^{-3}$ S/cm. The dashed line indicates the boundary between regimes II and III.

the different regimes are governed by the ratio $L_p\tilde{R}_k^{-1}/\sigma_{ion} = (L_p k^q/D^q)$: the transitions from regime I to regime II and from II to III are at ratios of ≈1000 and 1, respectively while regime IV becomes relevant for $L_p\tilde{R}_k^{-1}/\sigma_{ion} \ll L_p^2/h^2$.

The particle size L_p considerably influences the polarization resistance for high surface reaction rates (low $\tilde{R}_k$, regime I) while for increasing $\tilde{R}_k$-values the effect of L_p decreases. For each $\tilde{R}_k$-value a slope α can be calculated from the $\log(\tilde{R}_{pol})-\log(L_p)$ curve and this slope (which corresponds to the exponent α in $\tilde{R}_{pol}\propto L_p^{\alpha}$) is plotted in Fig. 4 for different k^q/D^q ratios. The α-factors again reflect, to a good approximation, the regimes mentioned above: $\alpha > 0.85$ for high k^q/D^q-values corresponds to regime I and thus to the case that the entire reduction reaction takes place close to the 3PB. A high 3PB length per area (i.e. a small particle size) can then strongly decrease the polarization resistance. The exponent $\alpha = 1/2$ for low k^q/D^q-values, on the other hand, reflects regime III with more than one particle layer being electrochemically active and the transition from $\alpha = 1/2$ to $\alpha > 0.85$ is equivalent to regime II in Fig. 3a.

Fig. 4 may be used to predict the geometry dependence of the polarization resistance for different materials. However, for many potential SOFC cathode materials k/D-values are only available from chemical diffusion or tracer experiments while here electrical driving forces and thus electrical k- and D-values are meant (cf. Ref [10]). Nevertheless, in Fig. 4b literature values from tracer experiments[11] (k^*/D^*) are included. If k^*/D^* is identical with k^q/D^q, $La_{0.8}Sr_{0.2}MnO_3$ is in regime II (only first particle layer active) while $La_{0.8}Sr_{0.2}CoO_3$ lies in regime III. Please note that the surface path of the oxygen reduction reaction (see Introduction) is neglected in this consideration which is certainly problematic for $La_{0.8}Sr_{0.2}MnO_3$.[12]

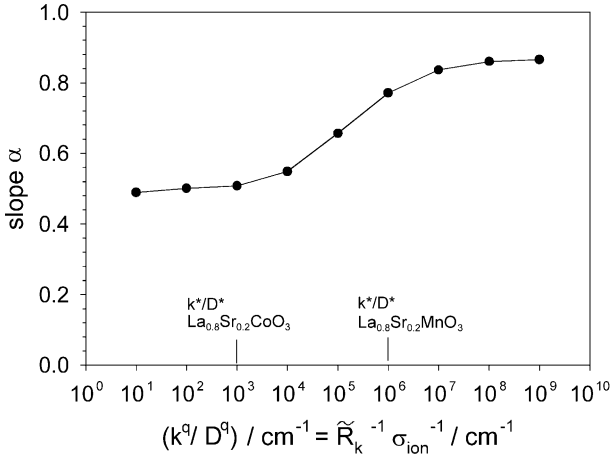

Fig. 4. Exponent α of the relation between polarization resistance and particle size ($\tilde{R}_{pol}\propto L_p^{\alpha}$) for different $\tilde{R}_k^{-1}/\sigma_{ion}$-ratios. Some data of tracer experiments (k^*/D^*)[11] are also indicated.

An interpolation formula which describes the polarization resistance of both geometries in the regimes I and II (i.e. $L_p k^q/D^q \geq 1$) surprisingly well reads

$$\tilde{R}_{pol} \approx \frac{L_p}{4\alpha\sigma_{ion}} + \frac{8}{\pi}\sqrt{\frac{\tilde{R}_k L_p}{\sigma_{ion}}} \quad (1)$$

with $\alpha = 1$. The first term in Eq. (2) reflects the situation of very fast oxygen reduction reaction at the cathode and thus corresponds to current flow mainly close to the 3PB. This term can therefore be expected to strongly depend on the exact shape of the 3PBs. "Wavy" or fractal-like 3PB-lines and larger particle densities enhance α and α-values of 2–4 are probably more realistic in porous SOFC cathodes (cf. Ref. [9]).

For $L_p k^q/D^q << 1$ it turns out that, at least for geometry A, the potential distributions are quasi-one-dimensional and analytical calculations similar to those reported for porous electrodes in liquid electrochemistry[13] are sensible. The solution of the corresponding differential equation $\partial^2\tilde{\mu}_V/\partial x^2 = 4(\tilde{\mu}_V - 2eU)/\left(L_p\sigma_{ion}\tilde{R}_k\right)$ leads to the area-related polarization resistance

$$\tilde{R}_{pol} = \frac{8}{\pi\sigma_{ion}}\sqrt{L_p\tilde{R}_k\sigma_{ion}}\coth\left(h\sqrt{\frac{4}{L_p\tilde{R}_k\sigma_{ion}}}\right). \quad (2)$$

As shown in Fig. 3b, Eq. (2) shows very good agreement with the numerical results in regimes III and IV of geometry A.

From Eqs. (1) and (2) one can therefore estimate which combinations of $\tilde{R}_k$, σ_{ion} and L_p might lead to reasonable SOFC cathodes with polarization resistances of the order of 0.15 Ωcm^2. These formulae are complementary to that derived from one-dimensional continuum electrode models in Refs. [6,7]: Eq. (1) can be used for large $k^q/D^q(=\tilde{R}_k^{-1}/\sigma_{ion})$ values (with only one particle layer being active) while the equations in Refs. [6,7] are valid only for comparably small k^q/D^q values. On the other hand, the continuum electrode models explicitly take account of the porosity of the cathode. A more detailed analysis and comparison with continuum electrode approaches will be given in a forthcoming paper.

4. Conclusions

Depending on the ratio of k^q/D^q $(=\tilde{R}_k^{-1}/\sigma_{ion})$ of a mixed conducting cathode, four regimes can be distinguished: For k^q/D^q-values much larger than the inverse particle size L_p (regime I) only small regions close to the three phase boundaries are relevant with respect to the oxygen reduction. A decreasing k^q/D^q ratio "activates" more and more of the cathode, i.e. the area of the MIEC surface which is involved in the oxygen reduction reaction monotonically increases: In

regime II ($L_p k^q/D^q$-values between 1 and 1000) it is still mainly the first particle layer which contributes to the oxygen reduction; $k^q L_p/D^q$-values <1 lead to a penetration of the ionic current into the cathode network (regime III) and finally the entire cathode surface is of importance (regime IV). Each regime exhibits a characteristic dependence of the polarization resistance on surface reaction coefficient, ionic conductivity and particle size. The ionic conductivity, for example, is most important in regimes I and II; the influence of the particle size decreases with increasing surface reaction resistance. The calculations yielded interpolation formulae which may be used to quantitatively estimate the polarization resistance of MIECs.

References

1. Siebert, E., Hammouche, A. and Kleitz, M., Impedance spectroscopy analysis of $La_{1-x}Sr_xMnO_3$-yttria-stabilized zirconia electrode kinetics. *Electrochim. Acta*, 1995, **40**, 1741–1753.
2. Mizusaki, J., Saito, T. and Tagawa, H., A chemical diffusion-controlled electrode reaction at the compact $La_{1-x}Sr_xMnO_3$/stabilized zirconia interface in oxygen atmospheres. *J. Electrochem. Soc.*, 1996, **143**, 3065–3073.
3. Endo, A., Ihara, M., Komiyama, H. and Yamada, K., Cathodic reaction mechanism for dense Sr-doped lanthanum manganite electrodes. *Solid State Ionics*, 1996, **86-88**, 1191–1195.
4. Steele, B. C. H., Survey of materials selection for ceramic fuel cells. 2. Cathodes and anodes. *Solid State Ionics*, 1996, **86-88**, 1223–1234.
5. Gharbage, B., Pagnier, T. and Hammou, A., Oxygen reduction at $La_{0.5}Sr_{0.5}MnO_3$ thin-film yttria-stabilized zirconia interface studied by impedance spectroscopy. *J. Electrochem. Soc.*, 1994, **141**, 2118–2121.
6. Adler, S. B., Lane, J. A. and Steele, B. C. H., Electrode kinetics of porous mixed-conducting oxygen electrodes. *J. Electrochem. Soc.*, 1996, **143**, 3554–3564.
7. Deng, H., Zhou, M. and Abeles, B., Diffusion-reaction in mixed ionic-electronic solid oxide membranes with porous electrodes. *Solid State Ionics*, 1994, **74**, 75–84.
8. Deng, H., Zhou, M. and Abeles, B., Transport in solid porous electrodes: Effect of gas diffusion. *Solid State Ionics*, 1995, **80**, 213–222.
9. Fleig, J., On the width of the electrochemically active region in mixed conducting solid oxide fuel cell cathodes. *J. Power Sources*, 2002, **105**, 228–238.
10. Maier, J., On the correlation of macroscopic and microscopic rate constants in solid state chemistry. *Solid State Ionics*, 1998, **112**, 197–228.
11. De Souza, R. A. and Kilner, J. A., Oxygen transport in $La_{1-x}Sr_xMn_{1-y}Co_yO_{3+/-delta}$ perovskites part II. Oxygen surface exchange. *Solid State Ionics*, 1999, **126**, 153–161.
12. Brichzin, V., Fleig, J., Habermeier, H.-U., Cristiani, G. and Maier, J., The geometry dependence of the polarization resistance of Sr-doped $LaMnO_3$ microelectrodes on yttria stabilized zirconia. *Solid State Ionics*, 2002, **152–153**, 499–507.
13. De Levie, R., On porous electrodes in electrolyte solutions IV. *Electrochim. Acta*, 1964, **9**, 1231–1245.